1-17-2024

Electron Trajectories and Critical Current in a Two-Dimensional Planar Magnetically Insulated Crossed-Field Gap

Xiaojun Zhu
Purdue University

Jack K. Wright
Purdue University

N. R. Sree Harsha
Purdue University

Jim Browning
Boise State University

Allen L. Garner
Purdue University

Publication Information

Zhu, Xiaojun; Wright, Jack K.; Harsha, N. R. S.; Browning, Jim; and Garner, Allen L. (2024). "Electron Trajectories and Critical Current in a Two-Dimensional Planar Magnetically Insulated Crossed-Field Gap". *IEEE Access, 12*, 11378-11387. https://doi.org/10.1109/ACCESS.2024.3355112

IEEE Access
Multidisciplinary | Rapid Review | Open Access Journal

Received 27 November 2023, accepted 11 January 2024, date of publication 17 January 2024, date of current version 25 January 2024.

Digital Object Identifier 10.1109/ACCESS.2024.3355112

RESEARCH ARTICLE

Electron Trajectories and Critical Current in a Two-Dimensional Planar Magnetically Insulated Crossed-Field Gap

XIAOJUN ZHU[1], (Graduate Student Member, IEEE), JACK K. WRIGHT[2], (Graduate Student Member, IEEE), N. R. SREE HARSHA[3], (Graduate Student Member, IEEE), JIM BROWNING[4], (Senior Member, IEEE), AND ALLEN L. GARNER[1,3,5], (Senior Member, IEEE)

[1]Elmore Family School of Electrical and Computer Engineering, Purdue University, West Lafayette, IN 47907, USA
[2]School of Aeronautics and Astronautics, Purdue University, West Lafayette, IN 47907, USA
[3]School of Nuclear Engineering, Purdue University, West Lafayette, IN 47907, USA
[4]Department of Electrical and Computer Engineering, Boise State University, Boise, ID 83725, USA
[5]Department of Agricultural and Biological Engineering, Purdue University, West Lafayette, IN 47907, USA

Corresponding author: Allen L. Garner (algarner@purdue.edu)

This work was supported in part by the Office of Naval Research under Grant N00014-21-1-2024, and in part by the Air Force Office of Scientific Research under Grant FA9550-22-1-0499.

ABSTRACT The critical current in a one-dimensional (1D) crossed-field gap is defined by the transition from a cycloidal flow to a near-Brillouin (nB) state characterized by electron flow orthogonal to both the electric and magnetic fields and uniform virtual cathode formation. Motivated by recent studies on space-charge-limited current in non-magnetic diodes, we assess the meaning of critical current in a magentically insulated two-dimensional (2D) planar crossed-field geometry. Particle-in-cell (PIC) simulations demonstrate that binary behavior between a laminar and turbulent state does not occur in 2D because the virtual cathode is nonuniform. Rather than a distinct nB state above the critical current as in 1D, there is an increase in Brillouin contribution with the presence of cycloidal components and noise even at low currents. To evaluate the electron flows in a 2D crossed-field gap in the absence of a binary transition, we developed two metrics to assess the Brillouin and cycloidal components in a 2D planar crossed-field gap for various emission widths and injection current densities by comparing the phase space plots from PIC simulations to analytical solutions for cycloidal and Brillouin flow. For a smaller emission width, less Brillouin contribution occurs for a given injection current, while maximizing the cycloidal noise requires a larger injection current. Once the virtual cathode starts to form and expand with increasing injection current, the cycloidal noise reaches its peak and then decreases while the Brillouin components become significant and increase.

INDEX TERMS Brillouin flow, cycloidal flow, crossed-field amplifiers (CFAs), crossed-field devices (CFDs), electron emission, high-power microwave, magnetrons, particle-in-cell, space-charge-limited current, vacuum tubes.

I. INTRODUCTION

Crossed-field devices (CFDs) with orthogonal electric and magnetic fields, such as magnetrons and crossed-field amplifiers (CFAs), have been widely used in many applications, including high-power microwave generation, radar systems, communication, plasma generation for semiconductor processing, and nuclear fusion [1], [2], [3], [4], [5], [6], [7], [8], [9]. CFDs often operate under magnetic insulation, meaning that an electron emitted from the cathode turns back

The associate editor coordinating the review of this manuscript and approving it for publication was Wenxin Liu.

to the cathode before reaching the anode [6]. Magnetic insulation requires that the transverse magnetic field B exceeds the threshold of the Hull cutoff magnetic field [10], given by

$$B_{\mathrm{H}} = \sqrt{\frac{2m_e V_{\mathrm{g}}}{eD^2} + \left(\frac{m_e v_0}{eD}\right)^2}, \tag{1}$$

where m_e and e are the electron mass and charge, respectively, V_{g} is the gap voltage, v_0 is the electron emission velocity, and D is the gap distance. This threshold corresponds to the magnetic field at which an electron emitted in the x-direction (parallel to the electric field and perpendicular to the magnetic field) reaches the anode with zero-velocity in the x-direction.

Another important condition for crossed-field devices is the Buneman-Hartree (BH) condition, which requires the velocity of the electrons at the top of the electron Brillouin flow hub to match the phase velocity of the radio frequency (RF) field [11]. The cavities on the anode (''slow-wave structure'' [4]) may be used to reduce the phase velocity of the RF field to ensure the BH condition or continuous synchronous interaction between the electrons and RF field for an oscillating state [6], [11]. Theoretical and simulation studies of planar CFDs are more mature than cylindrical CFDs due to their relative simplicity, despite the more common use of the latter geometry in practical applications [7]. Here, we focus on direct current (DC) CFDs in a planar geometry without cavities (e.g., with a smooth-bore anode [6]). These vacuum-based devices often operate in the space-charge-limited regime [12], [13] by extracting microwave power due to an inherent instability of the electron flows in the crossed-field gaps [14].

Electron flows in crossed-field gaps with various conditions have been studied in space-charge-limited regimes with or without magnetic insulation [2], [3], [15], [16], [17], [18], [19], [20], [21], [22], [23]. In some cases, the critical behavior of the electron flows under a certain condition can be described by modifying the classical Child-Langmuir (CL) law for space-charge limited current density (SCLCD) for a one-dimensional (1D), planar geometry, given by

$$J_{\mathrm{CL}} = (4\sqrt{2}/9)\varepsilon_0\sqrt{e/m_e}V_{\mathrm{g}}^{3/2}/D^2, \tag{2}$$

where ε_0 is the vacuum permittivity [24], [25]. When the crossed-magnetic field $B < B_{\mathrm{H}}$, electrons emitted from the cathode can reach the anode and the maximum permissible emitted current, referred to as the critical current J_{CR}, may be derived from first principles as a modification of J_{CL} [7], [21], [22], [23].

For $B = 0$, the critical current density is the SCLCD, which has been studied for different geometries [26], [27], [28], [29], multiple dimensions [30], [31], [32], [33], and nonzero initial velocity [33], [34]. The SCLCD (or critical current in the case of the crossed-field case) considering specific effects is often represented as a modification of J_{CL}. Multiple correction factors may be applied to (2) to incorporate the contributions of other physical phenomena, such as an orthogonal magnetic field [23], multiple dimensions, and nonzero initial velocity [33]. Introducing a magnetic field orthogonal to the electric field in the gap modifies the maximum emitted current density permissible to J_{CR}, which may be approximated as a crossed-field SCLCD (CF-SCLCD) [7].

If $B > B_H$, in which the electrons execute cycloidal orbits (without space-charge) and return to the cathode, a critical current J_{CR} may be found to mark the transition or collapse from a stationary cycloidal flow to the non-stationary near-Brillouin (nB) flow [3], [6], [23], [35]. The nB flow consists of the classical Brillouin flow [3], [16], [36] superimposed by a turbulent background characterized by virtual cathode (VC) oscillation [2], [3], [18], [19]. A crossed-field gap becomes more susceptible to nB flow under any slight perturbation, such as applying a small AC voltage across the gap in addition to the DC bias [17], adding an external series resistor [18], or introducing a component of the magnetic field parallel to the electric field (which additionally eliminates magnetic insulation for any B) [19]. Because all these conditions cause space-charge to buildup in the gap [18], [19], or VC formation right in front of the cathode [17], the electron trajectories eventually collapse to nB flow.

However, such a transition or collapse to the nB state may only occur when a *uniform* VC can be formed, such as in 1D [3], [7], [15], [17], [18], [19], [37] or two-dimensions (2D) with a crossed-magnetic field normal to the infinite direction (neglected depth) [23] (e.g., B is in the y-direction, as shown in Fig. 1). This resembles higher dimensional SCLCD problems where a nonuniform VC appears initially in a limited region [30], [33], [38]. The critical current density J_{CR} for 1D and 2D planar CFDs was found analytically by assuming a space-charge-limited condition and examined by electrostatic, particle-in-cell (PIC) simulation in the nonrelativistic regime [3], [23]. Note that this space-charge limited condition agreed reasonably well with the actual critical current derived separately for 1D [39]. The 1D theory was reproduced using variational calculus and extended to cylindrical geometry [7].

For a magnetic field applied parallel to the infinite direction (e.g., B aligns with the z-direction in Fig. 1), our 2D PIC simulations exhibit no complete and sudden collapses of cycloidal flow to an nB state as in 1D. Instead, for $J > J_{CR}$, the VC may only form in a limited region on the cathode, generating both cycloidal and Brillouin components. In fact, Brillouin components appear even for $J_{\mathrm{in}} \ll J_{\mathrm{CR,1D}}$ [3] for a large emission width with the contribution of the Brillouin components increasing with increasing J_{in}. A 3D simulation of electron perturbation induced by a magnetic field tilt also demonstrated no sudden collapse of cycloidal flow [20].

The absence of a transition in electron trajectory modality makes using either the cycloidal or Brillouin model alone to describe the electron beam impractical. Instead, in this work, we quantify the relative contributions of each individual mechanism to characterize the electron trajectories and relative stability. Partially inspired by Slater's orbits that generalize both cycloidal and Brillouin orbits [13], we developed

two metrics to assess the Brillouin and cycloidal components in a 2D planar crossed-field gap for various emission widths and injection current densities. We used the analytical solution of both Brillouin and cycloidal flows and 2D PIC simulation results to construct the metrics. We further studied VC formation and how the VC altered these metrics. While neither our metrics nor Slater's orbits describe an oscillating magnetron, they may elucidate the behavior in the oscillatory range [13]. Similar to the methods developed for analyzing oscillating magnetrons based on PIC data [40], the present assessments may be applied and extended to other similar devices or physical models, such as magnetically insulated line oscillators [16], two-species Brillouin flow [41], Hall thrusters [42], and Z-pinch [43].

Section II describes the model and PIC simulations for assessing the electron flows in a crossed-field gap. Section III discusses the results. We make concluding remarks in Section IV.

II. MODEL AND SIMULATION

A. MODEL PARAMETERS

We consider a crossed-field gap in a 2D planar geometry using XOOPIC (2D Object-Oriented Particle-in-Cell code [44]) with electrostatic and nonrelativistic settings. Fig. 1 shows the simulation geometry and parameters. The cathode was grounded at $x = 0$ and an anode was biased to V_g at $x = D$ with a magnetic field $\vec{B}$ in the $-z$-direction. For comparison, we used the device parameters based on the Navy Aegis CFA that was used in prior 1D crossed-field studies that determined the 1D critical current density $J_{CR,1D}$ that marks the transition from cycloidal flow to near-Brillouin (nB) flow [2], [3]. We fixed the gap distance $D = 0.00216$ m, magnetic field $B = 0.27$ T, bias voltage $V_g = 12$ kV, and electron injection energy of 0.5 eV (normal injection with initial velocity $v_0 \approx 0$), which gives $B/B_H = 1.579$ [3]. We set the length of the cathode $L = 8D$ with dielectric boundaries at $y = 0$ and $y = L$. While applying periodic boundary conditions at $y = 0$ and $y = L$ may resemble a pseudo-cylindrical crossed-field device, we focus on a planar crossed-field device here with dielectric boundaries that drain electrons. Electrons were emitted from $y = L$ to $y = L - W$, where W is the emission width. We selected emission from this region to ensure that electrons had adequate space (and, concomitantly, time) to complete a cycloidal orbit after emission. We recorded raw data from XOOPIC (such as electron number density and velocity profiles) after the number of macroparticles reached a steady-state with minimal variation (typically $< 5\%$ of the steady-state number). Note that applying periodic boundaries would cause the number of macroparticles to increase without bound rather than reach a steady state. The numerical settings, with a square mesh size with dimensions $\Delta x = \Delta y = 5.4 \times 10^{-5}$ m and a time step of $\Delta t = 9 \times 10^{-14}$s, are identical to our previous work [33] to ensure numerical stability [45].

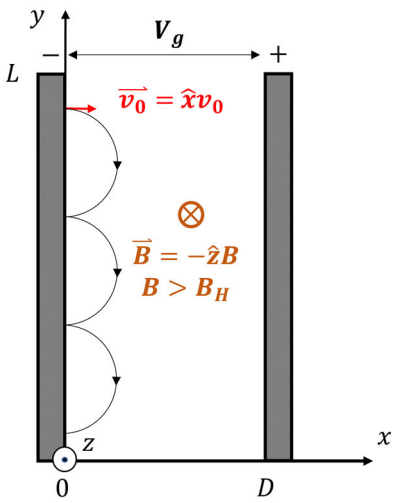

FIGURE 1. Schematic of a representative magnetically insulated crossed-field gap (magnetic field $B > B_H$, where B_H is the Hull cutoff magnetic field) used in the simulations with cycloidal electron trajectories (without space-charge). The grounded cathode from which electrons are emitted is at $x = 0$ and the anode at $x = D$, is held at a potential V_g. The dielectric boundaries, where the electrons are drained off, were set at $y = 0$ and $y = L$.

We used the analytical Brillouin flow solutions in 1D to evaluate the components of cycloidal, Brillouin, and cycloidal noise from XOOPIC models. We assume that electron flow consists only of these three components. The analytical velocity components for electrons in 1D Brillouin flow in the x- and y-directions are given by [4] and [13]

$$v_x(x) = 0 \tag{3}$$

and

$$v_y(x) = -\omega_c x, \tag{4}$$

respectively, where $\omega_c = eB/m_e$ is the electron cyclotron frequency. Note that (4) is identical to the analytical representation of cycloidal flow without space-charge. The number density for Brillouin flow, which is constant, is obtained by setting $\omega_c^2 = \omega_p^2 = e^2 n_b/(\varepsilon_0 m_e)$, where ω_p is the plasma frequency, and rearranging to obtain [4], [13]

$$n_b = \frac{B^2 \varepsilon_0}{m_e}. \tag{5}$$

B. BRILLOUIN COMPONENTS AND CYCLOIDAL NOISE

Fig. 2 shows the velocity in the x-direction at the p^{th} data point $v_x(x_p)$, where x_p is the displacement in the x-direction at the p^{th} data point, from XOOPIC compared to the analytical Brillouin flow solution of $v_x(x)$ from (3). Fig. 3 compares the velocity in the y-direction $v_y(x_p)$ from XOOPIC to the analytical Brillouin flow solution of $v_y(x)$ from (4).

Increasing J_{in} causes more particles to exhibit Brillouin-like behavior [i.e., $v_x(x_p) = 0$], as shown in Fig. 2(b), compared to the cycloidal orbit from Fig. 2(a). Although more particles exhibit Brillouin-like behavior, this buildup

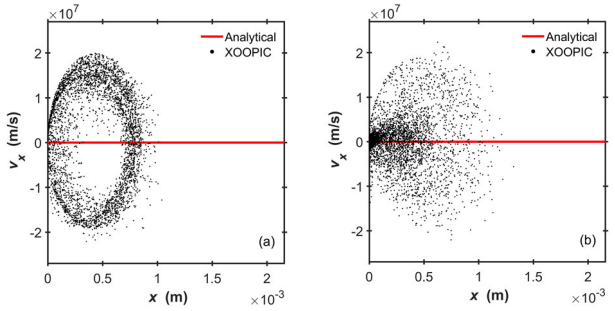

FIGURE 2. Electron velocity in the x-direction $v_x(x)$ from XOOPIC with injection current density J of (a) 5.79 × 10^4 A/m^2 ($J \ll J_{CR,1D}$, where $J_{CR,1D}$ is the 1D critical current density) and (b) 2.315 × 10^5 A/m^2 ($J > J_{CR,1D}$) compared to the analytical Brillouin flow velocity profile $v_x(x) = 0$ in red.

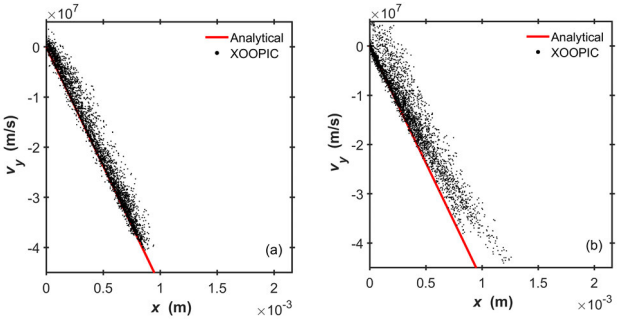

FIGURE 3. Electron velocity in the y-direction $v_y(x)$ from XOOPIC with injection current density of (a) 5.79 × 10^4 A/m^2 ($\ll J_{CR,1D}$, where $J_{CR,1D}$ is the 1D critical current density) and (b) 2.315 × 10^5 A/m^2 ($> J_{CR,1D}$) compared to the analytical Brillouin/cycloidal flow velocity profile $v_y(x) = -\omega_c x$ in red.

of space-charge with no (or little) velocity in the x-direction is insufficient to induce a complete collapse of the cycloidal orbit, as observed in previous 1D simulations for $J_{in} > J_{CR,1D}$ [3] or 2D simulations with $\vec{B}$ in the y-direction [23]. Note that assessing Brillouin components based on the analytical solution for Brillouin flow and PIC simulations is approximately equivalent to assessing near-Brillouin (nB) components. Ideal Brillouin flow is used as a theoretical approximation to the nB flow in simulations [35]. The Brillouin components that fully satisfy (3)-(5) cannot be separated from the nB components in 1D or 2D PIC simulations. The Brillouin components always coincide with a VC region (at $x \approx 0$) with a number density much higher than n_b in (5) both in 1D XPDP1 [2], [3], [46] and 2D XOOPIC [44] in this work. Our XPDP1 results that we report later show that the velocity profile of nB flow in 1D is identical to (3) [2], [3] and (4).

Fig. 3 shows that raising J_{in} also generally increases the cycloidal noise. Because Brillouin and cycloidal flow have identical $v_y(x)$ from (4), we cannot distinguish between them based on $v_y(x)$ alone. However, we can assess the cycloidal noise in the system by examining the relative difference between the analytical solution $v_y(x) = -\omega_c x$ and the PIC result $v_y(x_p)$, or defining $\Delta v_y(x_p) = v_y(x_p) - (-\omega_c x_p)$. Quantifying the relative contribution of Brillouin or cycloidal flow requires first calculating the fraction F of particles as a function of $v_x(x)$ and $\Delta v_y(x)$, respectively, with scaling/normalization using the number density in each case. Appendix summarizes the process for using MATLAB to determine F as a function of either $v_x(x)$ or $\Delta v_y(x)$ from the XOOPIC simulations.

Fig. 4 shows F as a function of $v_x(x)$ and $\Delta v_y(x)$ for various J_{in} with $W = 8D$. As J_{in} increases, the variation of F suggests more Brillouin components [with higher fraction F in $v_x \approx 0$ and $\Delta v_y(x) \approx 0$] and cycloidal noise [higher F in large $|\Delta v_y(x)|$] components. Fig. 4(a) exhibits "Brillouin peaks" in F for $v_x \approx 0$ for sufficiently high J_{in}, suggesting stronger "Brillouin-ness" in the electron flows. In general, the distributions of v_x for various J_{in} in Fig. 4(a) are symmetrical to $v_x = 0$, while the distributions of $\Delta v_y(x)$ are asymmetrical to $\Delta v_y(x) = 0$, as shown in Fig. 4(b). The latter indicates that more electrons have lower speeds, compared to (4), which corresponds to an analytical (or single particle) cycloidal trajectory or Brillouin flow, while traveling along the -y-direction but exhibit a higher maximum displacement in the x-direction in the presence of greater cycloidal noise, as shown in Fig. 3(b). This could be important to magnetron startup [40] according to the BH condition [11].

C. VIRTUAL CATHODE (VC) FORMATION

A VC may appear for sufficiently high J_{in}. Fig. 5 shows the potential $\phi(x, y)$ for various J_{in} with $W/D = 8$. For high J_{in}, the VC first appears where the newly emitted electrons interact with the returning electrons, creating a small space-charge-limited region, as shown from $0 < y \lesssim 0.012$ m in Fig. 5(b). From $\sim 0.012\text{m} \lesssim y < L$, there are no returning electrons, minimizing (or eliminating) the space-charge effect. For higher J_{in}, the VC would nonuniformly cover the entire emission region, as shown in Fig. 5(c). The nonuniformity of the VC formation as J_{in} increases may explain why cycloidal flow does not collapse to nB in 2D cases with B_z for $J_{in} \gg J_{CR,1D} = 2.1 \times 10^5$ A/m^2 [3] for large W/D, despite the asymmetry of the electron flows caused by the crossed B_z in our 2D geometry or in any 3D geometry. Note that we assume $J_{CR,2D,B_z} \approx J_{CR,1D}$ as $W/D \gg 1$, where $J_{CR,2D,B_z}$ is the 2D critical current density with an applied B_z.

This differs from 1D or 2D (with B_y) scenarios in which the returning electrons will *always* interact with the departing ones. In fact, both 1D and 2D theories considered the interaction of the returning and newly emitted electrons [3], [23]. Both $J_{CR,1D}$ and $J_{CR,2D}$ predict VC formation and mark the transition from cycloidal flow to nB flow. This raises the question of how the appearance of the VC would affect the electron flows in the 2D crossed-field gap with B_z considered here.

In our XOOPIC models, the 2D critical current density $J_{CR,2D,B_z}$ may only be determined by identifying the potential derivative $d\phi/dx = 0$ or the electric field $E_x = 0$ at $x = 0$, which corresponds to the SCLC for zero emission

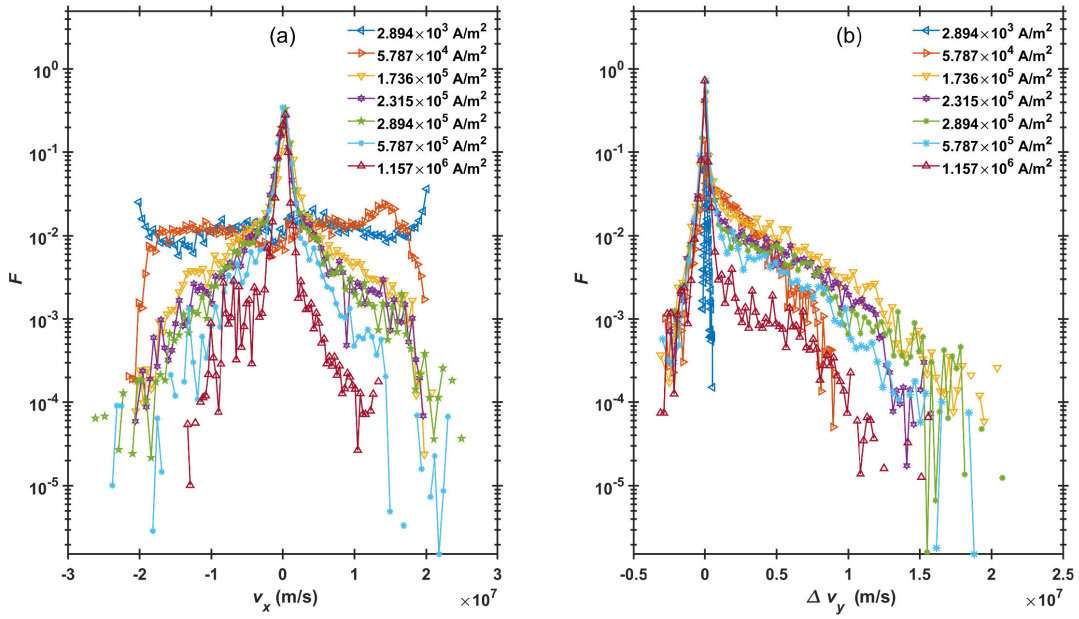

FIGURE 4. The fraction of particles F (dimensionless) for a given (a) $v_x(x_p)$ and (b) $\Delta v_y(x_p)$ for various injection current density with emission width $W = 8D$.

velocity [2]. A more practical way is to identify whether $E_x > 0$ at $x = 0$ by varying J_{in} in a binary search manner [33]. The resulting $J_{\text{CR,2D,B}_z}$ from XOOPIC is the minimum J_{in} that results in VC formation. We discuss the results in the next section.

Unlike our previous studies using XOOPIC for $B = 0$ [33] with extended regions near the dielectric boundaries, electrons may accumulate at the cell associated with $x = 0$ and $y = 0$ where the dielectric boundary (at $y = 0$) and Dirichlet boundary (at $x = 0$) intersect for $W/D = 8$, which is an intrinsic and inevitable numerical issue in XOOPIC for this calculation. This causes $E_x > 0$ at $x = 0$ and $y = 0$ even with low J_{in}. Thus, this false VC must be ignored when calculating $J_{\text{CR,2D,}B_z}$ from XOOPIC. In the next section, we will demonstrate that this does not significantly influence our assessment.

III. RESULTS AND DISCUSSION

To compare the results in Fig. 4 and other emission widths W, we further introduce two quantities C_B or C_T that serve as metrics, or figures of merit, for each curve to assess the Brillouin and cycloidal noise components, respectively. Specifically, we considered

$$C_B = \frac{1}{\langle (v_x(x_q))^2 \rangle} = \frac{1}{\sum_{q=1}^{N_q} \left\{ F\left(x_q\right) \left[v_x\left(x_q\right) \right]^2 \right\}}, \quad (6)$$

and

$$C_T = \langle (\Delta v_y(x_q))^2 \rangle = \sum_{q=1}^{N_q} \left\{ F\left(x_q\right) \left[\Delta v_y\left(x_q\right) \right]^2 \right\}, \quad (7)$$

where N_q is the number of the intervals (bins) of $v_x(x_q)$ or $\Delta v_y\left(x_q\right)$. Note that $\langle (v_x(x_q))^2 \rangle = \langle (v_x(x_p))^2 \rangle$ and $\langle (\Delta v_y(x_q))^2 \rangle = \langle (\Delta v_x(x_q))^2 \rangle$. Since $v_x \approx 0$ for Brillouin (or nB), we can use $\langle (\Delta v_y(x_q))^2 \rangle$ to evaluate the Brillouin components with smaller/larger values indicating greater Brillouin/cycloidal contributions. We define C_B as the reciprocal of this value to make it directly proportional to the "Brillouin-ness" of the flow. For C_T, since $v_y(x) = -\omega_c x$ for both Brillouin and cycloidal flow, a larger overall difference from this value [i.e., a larger $\langle (\Delta v_y(x_q))^2 \rangle$] indicates greater cycloidal noise. Equation (7) indicates that C_T is directly proportional to the cycloidal noise. Fig. 6 shows (a) C_B and (b) C_T for W/D =0.5, 1, 2, 4, and 8 as a function of J_{in} from XOOPIC and XPDP1 [2], [3], [46] simulations. We also examined the time-dependent behavior of C_B and C_T up to 8 ns. Both quantities reached steady states, as indicated by the number of macroparticles becoming stable with minimal variation.

For 1D XPDP1 simulations, C_B and C_T models the sudden change for $J_{\text{in}} = J_{\text{CR,1D}}$, corresponding to the transition from a stable cycloidal flow to the nB state, while the 2D results do not dramatically change behavior for $J_{\text{in}} \approx J_{\text{CR,2D}}$. Specifically, C_B increases gradually as J_{in} increases for 2D models. Although the methods of data processing of raw PIC data for XPDP1 and XOOPIC are similar, the two metrics from 1D or 2D PIC do not seem directly comparable due to the difference behavior at this transition.

Fig. 6(a) shows that for most 2D cases, C_B decreases with decreasing W for a given J_{in}. This resembles the results in 2D nonmagnetic cases [30], [33], [38], where the SCLCD for $W/D \lessapprox 1$ is much higher than those determined for either large W/D or 1D. For the crossed-field case, this occurs

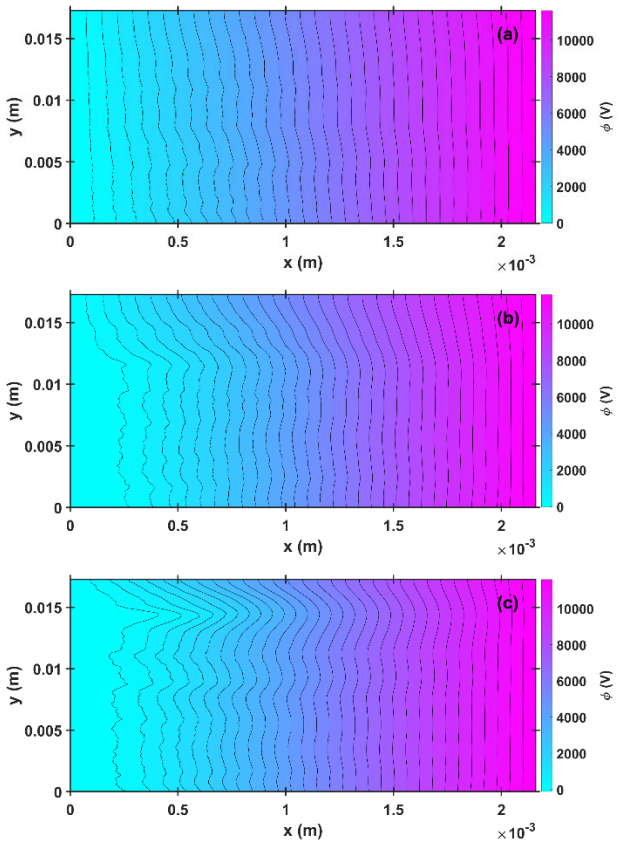

FIGURE 5. Potential $\phi(x, y)$ with $W/D = 8$ and injection current densities of (a) 5.79×10^4 A/m^2 without VC formation, (b) 1.74×10^5 A/m^2 with a VC from $0 < y0.012$ m where the newly emitted electrons interact with the returning electrons, and (c) 5.79×10^5 A/m^2 with a VC covering the entire emission region.

because VC formation for a smaller W/D requires a higher J_{in}, which increases the limiting current ($B < B_{\text{H}}$) or reduces the Brillouin components ($B > B_{\text{H}}$). Since Brillouin flow also arises due to VC formation, or space-charge buildup at the cathode [3], [17], [18], [19], similar to SCLCD, we anticipate similar behavior.

For smaller W, Fig. 6(b) shows that C_T also peaks and decreases at higher J_{in}, similar to VC formation. Thus, we conjecture that VC formation may affect the cycloidal noise, or C_{T}. Fig. 7 compares $J_{\text{CR,2D}}$ from XOOPIC to the injection current density $J_{\text{in,p}}$ associated with the maximum value of the metric C_{T} for each W/D considered. We obtained $J_{\text{CR,2D}}$ from XOOPIC by varying J_{in} until reaching the minimum value that caused VC formation such that further iterations induced negligible error [33]. When determining $J_{\text{in,p}}$ associated with the maximum C_{T}, we only obtained $J_{\text{in,p}}$ from our tested values of J_{in} without iterations.

We may also plot 2D semi-empirical and analytical $J_{\text{CR,2D}}$ [23], although they should be applicable only for B_{y}. We assume they both should provide reasonable estimates for B_z, at least for large W/D with zero initial velocity, similar to $B < B_{\text{H}}$ [23]. The semi-empirical form of $J_{\text{CR,2D}}$, similar to the semi-empirical 2D uniform SCLC for $v_0 \neq 0$ and $B = 0$ [33], is given by

$$J_{\text{CR,2D}} = J_{\text{CL}} p(B, V_g, D) f(W/D), \tag{8}$$

where the field correction factor [3] is given by

$$p\left(B, V_g, D\right) = \frac{9}{8\pi}\left(\frac{B}{B_{\text{H}}}\right)^3\left[1-\sqrt{1-\left(\frac{B_{\text{H}}}{B}\right)}\right] \tag{9}$$

and the geometry correction factor [30] is given by

$$f\left(\frac{W}{D}\right) = \left[1+\frac{1}{\pi W/D}\right]. \tag{10}$$

Note that the *exact* solution for the 1D crossed-field case is $J_{\text{CR,1D}} = J_{\text{CL}} p\left(B, V_g, D\right)$ [3]. The semi-empirical form in (8) is obtained simply by multiplying J_{CL} from (2) by the two correction factors from (9) and (10). This is based on a conjuncture that additional effects that contribute to SCLC may be considered as multiplicative correction factors to J_{CL} for rapid estimates, which we have shown is reasonable for nonmagnetic cases with sufficiently low v_0 [33]. Fig. 7 shows that such a semi-empirical form gives similar values compared to the theoretical $J_{\text{CR,2D}}$ [23]. However, at smaller W/D, the semi-empirical relationship deviates from the theory, similar to 2D uniform SCLCD with nonzero v_0 [33].

TABLE 1. Estimated C_{B} associated with $J_{\text{CR,2D}}$ from XOOPIC for each W/D using linear interpolation from the results in Fig. 6(a).

W/D	0.5	1	2	4	8
C_{B} $[10^{-14}\text{s}^2\text{m}^{-2}]$	1.3134	1.5832	1.4298	1.6706	1.7575

Both the semi-empirical and theoretical $J_{\text{CR,2D}}$ disagree with $J_{\text{CR,2D}}$ obtained from XOOPIC, even for relatively large W/D in which the returning electrons will interact with the departing ones. 1D and 2D theories typically assume that the returning and departing electrons interact [2], [3], [23]. The $J_{\text{CR,2D}}$ from XOOPIC follows a similar trend as (and agrees reasonably well with) $J_{\text{in,p}}$ obtained using the maximum value of C_{T}. Thus, we speculate that the cycloidal noise reaches a maximum and starts to decrease as the VC starts to form and expand along the cathode, as shown in Fig. 7. Fitting $J_{\text{CR,2D}}$ from XOOPIC and $J_{\text{in,p}}$ using $J = a\left(W/D\right)^b$ gives $a = 3.44\times10^5$ A/m^2 and $b = -0.5679$ for $J_{\text{CR,2D}}$ from XOOPIC (with $R^2 = 0.9814$) and $a = 4.14\times10^5$ A/m^2 and $b = -0.5418$ for $J_{\text{in,p}}$ (with $R^2 = 0.9749$) as the best-fit parameters.

In addition, since $J_{\text{CR,2D}}$ marks the appearance of a VC for each W/D, we may estimate C_{B} by applying linear interpolation to the results in Fig. 6(a). Table 1 shows similar C_{B} ($\sim1.5\times10^{-14}\text{s}^2\text{m}^{-2}$) associated with $J_{\text{CR,2D}}$ from XOOPIC for each W/D. This indicates that the Brillouin components are similar for each W upon VC formation, although $J_{\text{CR,2D}}$ varies for different W/D. It also shows the charge accumulation issue that arises due to the intersection of the planes for

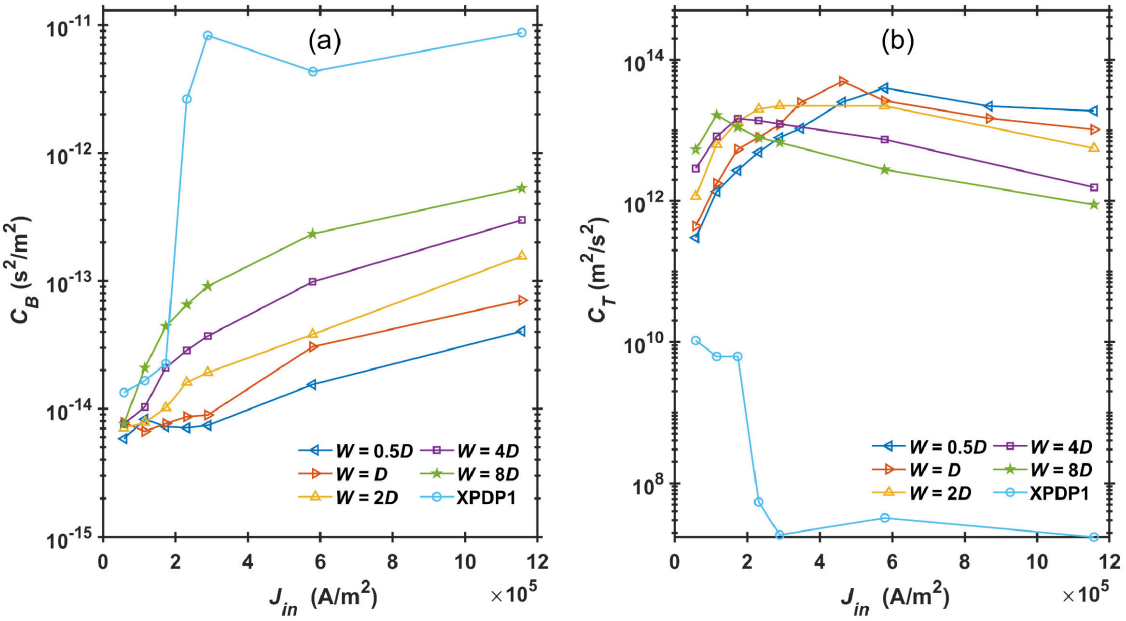

FIGURE 6. Brillouin components and cycloidal noise assessments: (a) C_B and (b) C_T as a function of injection current density J_{in} for $W = 0.5D$, D, $2D$, $4D$, $8D$ and 1D models from XPDP1.

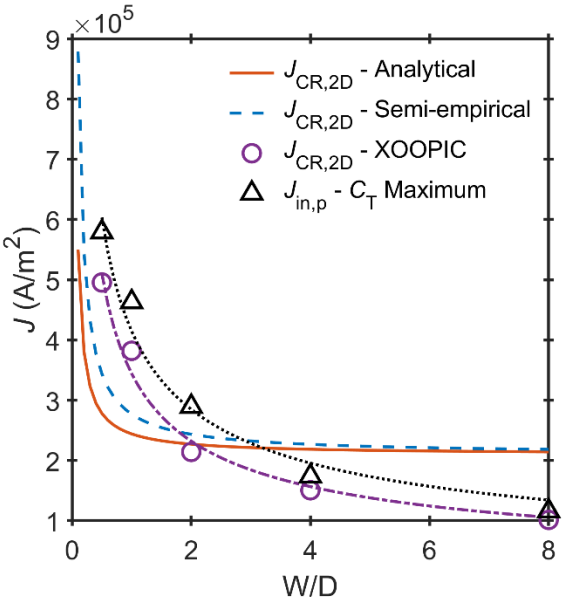

FIGURE 7. Comparison of the 2D critical current density $J_{\text{CR,2D}}$ from the analytical form [23], the semi-empirical equation (8), PIC, and the injection current density $J_{\text{in,p}}$ associated with the maximum value of C_T for assessing cycloidal noise as shown in Fig. 5(b). We fit $J_{\text{CR,2D}}$ from XOOPIC and $J_{\text{in,p}}$ using $J = a\,(W/D)^b$, where a and b are fitting parameters. We obtained $a = 3.44\times10^5$ A/m^2 and $b = -0.5679$ for $J_{\text{CR,2D}}$ from XOOPIC (with $R^2 = 0.9814$) and $a = 4.14\times10^5$ A/m^2 and $b = -0.5418$ for $J_{\text{in,p}}$ (with $R^2 = 0.9749$) as the best-fit parameters.

the Dirichlet and Neumann boundary conditions for $W/D = 8$ does not appreciably affect the evaluation of $J_{\text{CR,2D}}$ in XOOPIC. Furthermore, for $J_{\text{in}} > J_{\text{CR,2D}}$, the rate of change of C_{B} and C_{T} with respect to J_{in} eventually becomes essentially the same (“similar slope”) for each emission width after VC expansion. Although we have shown that $J_{\text{CR,2D}}$ may not be used to describe the electron flows in 2D crossed-field gaps where there is not binary behavior (i.e., a direct transition from cycloidal flow to nB flow upon exceeding a threshold critical current density), the formation of the VC associated with $J_{\text{CR,2D}}$ may still significantly affect the variations of Brillouin and cycloidal noise components.

IV. CONCLUSION

In 2D crossed-field gaps (CFGs), while the critical current density still characterizes the appearance of a VC, it no longer signifies the transition from stationary cycloidal flow to the nB state observed in 1D. Instead, Brillouin components coexist with cycloidal flows and noise, even for $J_{\text{in}} \ll J_{\text{CR,2D}}$. In this study, we developed two metrics for evaluating the components of near-Brillouin and cycloidal noise components in a 2D planar CFG with various W/D and J_{in}.

The metrics rely on data obtained from 2D PIC simulations and analytical solutions for cycloidal and Brillouin flow. For smaller W/D, Brillouin flow contributes less to the beam for a given J_{in}. Cycloidal noise initially increases with increasing J_{in} and VC formation before reaching a peak and decreasing. Furthermore, the Brillouin components behave similarly across W/D upon VC formation, although $J_{\text{CR,2D}}$ varies with W/D. The assessments potentially connect the newly developed metrics and the traditionally used critical current density for VC formation and transition to nB state for $B > B_{\text{H}}$ in 1D [2], [3], [7], [17], [19] or 2D with B_y [23]. Moreover, the presented methodology of assessing the

electron flow may be applied and extended to other crossed-field devices [16], [41], [42], [43].

Future work may assess the effect of secondary emission and/or multiple cycloids for a CFG. Future work may also consider a cylindrical CFG (or a planar one with periodic boundary conditions), two-species Brillouin [41], and collisional CFGs [47] (e.g., the role of ions in CFDs [15], [48]) flow, which become important in devices with imperfect vacuum that may undergo gap closure. Additionally, measuring the frequency of virtual cathode oscillation [3] as a function of emission width or emission energy in a 2D CFG may further elucidate the source of noise in CFDs [2].

APPENDIX
DATA PROCESSING

Take F as a function of $v_x(x)$ for example. We first construct $n\,(x_i)$ by integrating the discrete number density $n(x_i, y_j)$ from XOOPIC in the y-direction to obtain

$$n\,(x_i) = \frac{1}{L}\left[\sum\nolimits_{j=1}^{N_y} n\left(x_i, y_j\right)\Delta y\right], \tag{A-1}$$

where N_y is the number of cells in the y-direction, Δy is the cell size in the y-direction, i is the ith cell in the x-direction, j is the jth cell in the y-direction, and $L = N_y\Delta y$ is the length of the cathode. We may also write $n\,(x_i) = \left[\sum_{j=1}^{N_y} n\left(x_i, y_j\right)\right]/N_y$. We have far fewer cells in the x-direction N_x (e.g., 40) than the number of data points N_{ux} (e.g., $> 10^4$) of the numerical result $v_x(x_p)$ from XOOPIC, where p represents the pth data point in $v_x(x_p)$. Here, N_{ux} is independent of the number of cells, but it is inversely proportional to the particle power weight in the PIC models (or the number of the macroparticles). Since $n\,(x_i)$ is relatively not smooth, we use linear interpolation to construct $n\left(x_p\right)$, which has the same number of data points as N_{ux}. Each data point in $v_x(x_p)$ now corresponds to its associated $n\left(x_p\right)$. Then, each intermediate fraction f associated with such a data point can be determined by

$$f\left(x_p\right) = \frac{\int_{V'} n(x_p)dV'}{\sum_{p=1}^{N_{ux}}\int_{V'} n(x_p)dV'}, \tag{A-2}$$

where V' is the volume of the simulation region. With discrete values, (A-2) would yield $f\left(x_p\right) = n(x_p)/\sum_{p=1}^{N_{ux}} n(n_p)$, where $\sum_{p=1}^{N_{ux}} f(n_p) = 1$. Each data point in $v_x(x_p)$ now corresponds to its associated $f\left(x_p\right)$. Next, we construct the final normalized fraction $F(x_q)$ as a function of $v_x(x_q)$ with intervals, $v_x\left(x_{q+1}\right) - v(x_q)$, where q represents the qth bin. Each discrete $F(x_q)$ is the sum of all $f\left(x_p\right)$ with its corresponding $v_x(x_p)$ located in the qth interval or bin, making $\sum_q F\left(x_q\right) = 1$. The relationship between $F(x_q)$ and $\Delta v_y(x_p)$ can be obtained in a similar manner.

ACKNOWLEDGMENT

The authors thank John Luginsland for helpful discussions.

REFERENCES

[1] D. Andreev, A. Kuskov, and E. Schamiloglu, "Review of the relativistic magnetron," *Matter Radiat. Extremes*, vol. 4, no. 6, Nov. 2019, Art. no. 067201, doi: 10.1063/1.5100028.

[2] P. J. Christenson, "Equilibrium, stability, and turbulence in cycloidal electron flows in crossed electric and magnetic fields," Ph.D. thesis, Dept. Nucl. Eng. Radiol. Sci., Univ. Michigan, Ann Arbor, MI, USA, 1996.

[3] P. J. Christenson and Y. Y. Lau, "Transition to turbulence in a crossed-field gap," *Phys. Plasmas*, vol. 1, no. 12, pp. 3725–3727, Dec. 1994, doi: 10.1063/1.870915.

[4] D. H. Simon, Y. Y. Lau, G. Greening, P. Wong, B. W. Hoff, and R. M. Gilgenbach, "Stability of Brillouin flow in planar, conventional, and inverted magnetrons," *Phys. Plasmas*, vol. 22, no. 8, Aug. 2015, Art. no. 082104, doi: 10.1063/1.4927798.

[5] J. C. Slater, *Microwave Electronics*, no. 3. New York, NY, USA: Dover, 1950.

[6] D. H. Simon, "Equilibrium and stability of Brillouin flow in planar, conventional, and inverted magnetrons," Ph.D. thesis, Dept. Nucl. Eng. Radiol. Sci., Univ. Michigan, Ann Arbor, MI, USA, 2015.

[7] A. M. Darr, R. Bhattacharya, J. Browning, and A. L. Garner, "Space-charge limited current in planar and cylindrical crossed-field diodes using variational calculus," *Phys. Plasmas*, vol. 28, no. 8, Aug. 2021, Art. no. 082110, doi: 10.1063/5.0054307.

[8] J. Browning, S. Fernandez-Gutierrez, M. C. Lin, D. N. Smithe, and J. Watrous, "Phase control and fast start-up of a magnetron using modulation of an addressable faceted cathode," *Appl. Phys. Lett.*, vol. 104, no. 23, Jun. 2014, Art. no. 233507.

[9] V. Nallasamy, S. K. Datta, S. U. Reddy, and P. K. Jain, "Advances and present trends in magnetically insulated line oscillator," *J. Electromagn. Waves Appl.*, vol. 31, no. 17, pp. 1864–1874, Nov. 2017, doi: 10.1080/09205071.2017.1338622.

[10] A. W. Hull, "The effect of a uniform magnetic field on the motion of electrons between coaxial cylinders," *Phys. Rev.*, vol. 18, no. 1, pp. 31–57, Jul. 1921, doi: 10.1103/PhysRev.18.31.

[11] G. J. Telkamp, "Note to users," *Itinerario*, vol. 5, nos. 3–4, pp. 68–69, Nov. 1981, doi: 10.1017/S0165115300023299.

[12] A. L. Garner, A. M. Loveless, J. N. Dahal, and A. Venkattraman, "A tutorial on theoretical and computational techniques for gas breakdown in microscale gaps," *IEEE Trans. Plasma Sci.*, vol. 48, no. 4, pp. 808–824, Apr. 2020, doi: 10.1109/TPS.2020.2979707.

[13] J. C. Slater, *Microwave Electronics*. New York, NY, USA: Van Nostrand, 1950.

[14] O. Buneman, R. H. Levy, and L. M. Linson, "Stability of crossed-field electron beams," *J. Appl. Phys.*, vol. 37, no. 8, pp. 3203–3222, Jul. 1966, doi: 10.1063/1.1703185.

[15] B. S. Stutzman and J. W. Luginsland, "Loss of magnetic insulation in a crossed-field diode: Ion and collisional effects," *IEEE Trans. Plasma Sci.*, vol. 38, no. 8, pp. 2010–2015, Aug. 2010, doi: 10.1109/TPS.2010.2051460.

[16] Y. Y. Lau, D. A. Packard, C. J. Swenson, J. W. Luginsland, D. Li, A. Jassem, N. M. Jordan, R. D. McBride, and R. M. Gilgenbach, "Explicit Brillouin flow solutions in magnetrons, magnetically insulated line oscillators, and radial magnetically insulated transmission lines," *IEEE Trans. Plasma Sci.*, vol. 49, no. 11, pp. 3418–3437, Nov. 2021, doi: 10.1109/TPS.2021.3092606.

[17] P. J. Christenson and Y. Y. Lau, "One-dimensional modulational instability in a crossed-field gap," *Phys. Rev. Lett.*, vol. 76, no. 18, pp. 3324–3327, Apr. 1996, doi: 10.1103/PhysRevLett.76.3324.

[18] P. J. Christenson, D. P. Chernin, A. L. Garner, and Y. Y. Lau, "Resistive destabilization of cycloidal electron flow and universality of (near-) Brillouin flow in a crossed-field gap," *Phys. Plasmas*, vol. 3, no. 12, pp. 4455–4462, Dec. 1996, doi: 10.1063/1.872064.

[19] A. L. Garner, Y. Y. Lau, and D. Chernin, "Collapse of cycloidal electron flows induced by misalignments in a magnetically insulated diode," *Phys. Plasmas*, vol. 5, no. 6, pp. 2447–2453, Jun. 1998, doi: 10.1063/1.872921.

[20] R. Bhattacharya, A. M. Darr, A. L. Garner, and J. Browning, "Analysis of injected electron beam propagation in a planar crossed-field gap," *Appl. Sci.*, vol. 11, no. 6, Mar. 2021, Art. no. 2540, doi: 10.3390/app11062540.

[21] Y. Y. Lau, P. J. Christenson, and D. Chernin, "Limiting current in a crossed-field gap," *Phys. Fluids B, Plasma Phys.*, vol. 5, no. 12, pp. 4486–4489, Dec. 1993, doi: 10.1063/1.860563.

[22] L. K. Ang, T. J. T. Kwan, and Y. Y. Lau, "Limiting current density in a crossed-field nanogap," *Phys. Rev. E, Stat. Phys. Plasmas Fluids Relat. Interdiscip. Top.*, vol. 64, no. 1, Jun. 2001, Art. no. 017501, doi: 10.1103/PhysRevE.64.017501.
[23] W. S. Koh and L. K. Ang, "Two-dimensional space-charge-limited flows in a crossed-field gap," *Appl. Phys. Lett.*, vol. 90, no. 14, Apr. 2007, Art. no. 141503, doi: 10.1063/1.2720710.
[24] P. Zhang, Á. Valfells, L. K. Ang, J. W. Luginsland, and Y. Y. Lau, "100 years of the physics of diodes," *Appl. Phys. Rev.*, vol. 4, no. 1, Mar. 2017, Art. no. 011304, doi: 10.1063/1.4978231.
[25] C. D. Child, "Discharge from hot CAO," *Phys. Rev., Ser. I*, vol. 32, no. 5, pp. 492–511, May 1911, doi: 10.1103/PhysRevSeriesI.32.492.
[26] I. Langmuir and K. B. Blodgett, "Currents limited by space charge between coaxial cylinders," *Phys. Rev.*, vol. 22, no. 4, pp. 347–356, Oct. 1923, doi: 10.1103/PhysRev.22.347.
[27] I. Langmuir and K. B. Blodgett, "Currents limited by space charge between concentric spheres," *Phys. Rev.*, vol. 24, no. 1, pp. 49–59, Jul. 1924, doi: 10.1103/PhysRev.24.49.
[28] A. L. Garner, A. M. Darr, and N. R. S. Harsha, "A tutorial on calculating space-charge-limited current density for general geometries and multiple dimensions," *IEEE Trans. Plasma Sci.*, vol. 50, no. 9, pp. 2528–2540, Sep. 2022, doi: 10.1109/TPS.2022.3172424.
[29] Y. B. Zhu, P. Zhang, A. Valfells, L. K. Ang, and Y. Y. Lau, "Novel scaling laws for the Langmuir–Blodgett solutions in cylindrical and spherical diodes," *Phys. Rev. Lett.*, vol. 110, no. 26, Jun. 2013, Art. no. 265007, doi: 10.1103/PhysRevLett.110.265007.
[30] Y. Y. Lau, "Simple theory for the two-dimensional child-Langmuir law," *Phys. Rev. Lett.*, vol. 87, no. 27, Dec. 2001, Art. no. 278301, doi: 10.1103/PhysRevLett.87.278301.
[31] N. R. Sree Harsha, M. Pearlman, J. Browning, and A. L. Garner, "A multi-dimensional Child–Langmuir law for any diode geometry," *Phys. Plasmas*, vol. 28, no. 12, Dec. 2021, Art. no. 122103, doi: 10.1063/5.0071018.
[32] A. Rokhlenko and J. L. Lebowitz, "Space-charge-limited 2D electron flow between two flat electrodes in a strong magnetic field," *Phys. Rev. Lett.*, vol. 91, no. 8, Aug. 2003, Art. no. 085002, doi: 10.1103/PhysRevLett.91.085002.
[33] X. Zhu, N. R. Sree Harsha, and A. L. Garner, "Uniform space-charge-limited current for a two-dimensional planar emitter with nonzero monoenergetic initial velocity," *J. Appl. Phys.*, vol. 134, no. 11, Sep. 2023, Art. no. 113301, doi: 10.1063/5.0167802.
[34] J. B. Huang, R. H. Yao, P. Zhao, and Y. B. Zhu, "Simulation of space-charge-limited current for hot electrons with initial velocity in a vacuum diode," *IEEE Trans. Electron Devices*, vol. 68, no. 7, pp. 3604–3610, Jul. 2021, doi: 10.1109/TED.2021.3085164.
[35] K. L. Cartwright, P. J. Christenson, J. P. Verboncoeur, and C. K. Birdsall, "Surface wave enhanced collisionless transport in a bounded crossed-field non-neutral plasma," *Phys. Plasmas*, vol. 7, no. 5, pp. 1740–1745, May 2000, doi: 10.1063/1.873993.
[36] L. Brillouin, "A theorem of Larmor and its importance for electrons in magnetic fields," *Phys. Rev.*, vol. 67, nos. 7–8, pp. 260–266, Apr. 1945, doi: 10.1103/PhysRev.67.260.
[37] A. M. Darr and A. L. Garner, "Modifications of limiting current and magnetic insulation in a crossed-field diode by a series resistor," *IEEE Access*, vol. 10, pp. 60438–60446, 2022, doi: 10.1109/ACCESS.2022.3180739.
[38] J. W. Luginsland, Y. Y. Lau, and R. M. Gilgenbach, "Two-dimensional child-langmuir law," *Phys. Rev. Lett.*, vol. 77, no. 22, pp. 4668–4670, Nov. 1996.
[39] P. J. Christenson and Y. Y. Lau, "Erratum: Transition to turbulence in a crossed-field gap," *Phys. Plasmas*, vol. 3, no. 11, p. 4293, Nov. 1996.
[40] A. Yue and J. Browning, "Electron population analysis techniques for understanding fundamental cross-field electron device physics," *IEEE Trans. Plasma Sci.*, vol. 50, no. 6, pp. 1775–1780, Jun. 2022, doi: 10.1109/TPS.2022.3172564.
[41] A. M. Darr and K. L. Cartwright, "Mutually magnetically insulated two-species Brillouin flow," *Phys. Plasmas*, vol. 30, no. 5, May 2023, Art. no. 053105, doi: 10.1063/5.0145768.
[42] M. Keidar, I. D. Boyd, and I. I. Beilis, "Plasma flow and plasma-wall transition in Hall thruster channel," *Phys. Plasmas*, vol. 8, pp. 5315–5322, 2001, doi: 10.1063/1.1421370.
[43] M. G. Haines, "A review of the dense Z-pinch," *Plasma Phys. Controlled Fusion*, vol. 53, no. 9, Sep. 2011, Art. no. 093001, doi: 10.1088/0741-3335/53/9/093001.
[44] J. P. Verboncoeur, A. B. Langdon, and N. T. Gladd, "An object-oriented electromagnetic PIC code," *Comput. Phys. Commun.*, vol. 87, nos. 1–2, pp. 199–211, 1995, doi: 10.1016/0010-4655(94)00173-Y.
[45] V. Vahedi, G. DiPeso, C. K. Birdsall, M. A. Lieberman, and T. D. Rognlien, "Capacitive RF discharges modelled by particle-in-cell Monte Carlo simulation. I. Analysis of numerical techniques," *Plasma Sources Sci. Technol.*, vol. 2, no. 4, pp. 261–272, Nov. 1993, doi: 10.1088/0963-0252/2/4/006.
[46] J. P. Verboncoeur, M. V. Alves, V. Vahedi, and C. K. Birdsall, "Simultaneous potential and circuit solution for 1D bounded plasma particle simulation codes," *J. Comput. Phys.*, vol. 102, no. 2, p. 424, Oct. 1992.
[47] A. L. Garner, A. M. Komrska, L. I. Breen, A. M. Loveless, and K. L. Cartwright, "Electron trajectories in a collisional crossed-field gap," *Appl. Phys. Lett.*, vol. 122, no. 19, May 2023, Art. no. 194101, doi: 10.1063/5.0147252.
[48] Y. Y. Lau, J. W. Luginsland, K. L. Cartwright, and M. D. Haworth, "Role of ions in a crossed-field diode," *Phys. Rev. Lett.*, vol. 98, no. 1, Jan. 2007, Art. no. 015002, doi: 10.1103/PhysRevLett.98.015002.

XIAOJUN ZHU (Graduate Student Member, IEEE) received the B.S. degree in applied physics from the Chengdu University of Technology, Chengdu, China, in 2016, and the M.S. degree in nuclear engineering from Purdue University, West Lafayette, IN, USA, in 2019, where he is currently pursuing the Ph.D. degree in electrical and computer engineering. His research interests include electromagnetic and multiphysics modeling, plasma physics, and RF/plasma engineering.

JACK K. WRIGHT (Graduate Student Member, IEEE) received the B.S. degree in aeronautics and astronautics from Purdue University, West Lafayette, IN, USA, in 2022, where he is currently pursuing the M.S. degree in aeronautics and astronautics. His research interests include crossed-field physics, space-charge-limited emission, and plasma dynamics.

N. R. SREE HARSHA (Graduate Student Member, IEEE) received the B.E. degree in electrical and electronics engineering from the Rashtreeya Vidyalaya College of Engineering, India, and the M.Sc. degree in nuclear science and engineering from the University of Bristol, U.K. He is currently pursuing the Ph.D. degree in nuclear engineering with the BioElectrics and ElectroPhysics Laboratory, Purdue University, West Lafayette, IN, USA. He is the coauthor of the book *The Foundations of Electric Circuit Theory* (IOP Publishing Ltd., 2016). His research interests include field and space-charge-limited emission, nanosecond pulsed discharges, plasma physics applications, high-power microwave generation, and entropy production principles.

JIM BROWNING (Senior Member, IEEE) received the B.S. and M.S. degrees in nuclear engineering from the Missouri School of Science and Technology, Rolla, MO, USA, in 1983 and 1985, respectively, and the Ph.D. degree from the University of Wisconsin–Madison, Madison, WI, USA, in 1988. He was a Consultant of emission technology and a Senior Development Engineer with PixTech, Inc., Montpellier, France, and Micron Technology, Inc., Boise, ID, USA. He joined Boise State University, Boise, ID, USA, in 2006, where he is currently a Professor with the Department of Electrical and Computer Engineering and the Associate Dean for Research with the College of Engineering. His current research interests include vacuum electron devices and cold atmospheric pressure plasma.

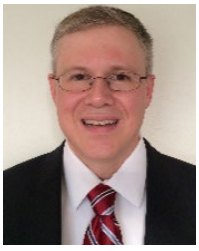

ALLEN L. GARNER (Senior Member, IEEE) received the B.S. degree (Hons.) in nuclear engineering from the University of Illinois at Urbana–Champaign, in 1996, the M.S.E. degree in nuclear engineering from the University of Michigan, Ann Arbor, in 1997, the M.S. degree in electrical engineering from Old Dominion University, Norfolk, VA, USA, in 2003, and the Ph.D. degree in nuclear engineering from the University of Michigan, in 2006.

From December 1997 to December 2003, he served as an active duty Naval officer onboard the USS Pasadena (SSN 752) and an instructor of the Prospective Nuclear Engineering Officer Course, Submarine Training Facility, Norfolk. From 2006 to 2012, he was an Electromagnetic Physicist with the GE Global Research Center, Niskayuna, NY, USA. In August 2012, he joined the School of Nuclear Engineering, Purdue University, West Lafayette, IN, USA, where he is currently a Professor and the Undergraduate Program Chair. He is also a Captain with the Navy Reserves and the Commanding Officer of NR SurgeMain Puget Sound Naval Shipyard Kitsap, Bremerton, WA, USA. His research interests include electron emission, gas breakdown, high-power microwaves, and biomedical applications of pulsed power and plasmas.

Prof. Garner is a member of the IEEE International Power Modulator and High Voltage Conference (IPMHVC) Executive Committee and the Dielectrics and Electrical Insulation Society Administrative Committee. He received the 2016 IEEE Nuclear and Plasma Sciences Early Achievement Award, the two Meritorious Service Medals, the Navy and Marine Corps Commendation Medal, and five Navy and Marine Corps Achievement Medals. He served as the Technical Program Chair for the 2016 IEEE IPMHVC, the Treasurer for the 2018 IEEE IPMHVC, and the Technical Program Chair for the 2022 IEEE IPMHVC. He is the General Conference Chair of the 2024 IEEE IPMHVC. He is a Licensed Professional Engineer in Michigan.